REPORT DOCUMENTATION PAGE

Form Approved
OMB No. 0704-0188

1. REPORT DATE *(DD-MM-YYYY)*	**2. REPORT TYPE**	**3. DATES COVERED** *(From - To)*
06 October 2015	Journal Article	12 May 2015 – 06 Oct 2015

4. TITLE AND SUBTITLE
A Tightly Coupled Non-Equilibrium Magneto-Hydrodynamic Model for Inductively Coupled RF Plasmas

5a. CONTRACT NUMBER

5b. GRANT NUMBER

5c. PROGRAM ELEMENT NUMBER

6. AUTHOR(S)
A. Munafo, S.A. Alfuhaid, J.-L. Cambier, M. Panesi

5d. PROJECT NUMBER

5e. TASK NUMBER

5f. WORK UNIT NUMBER
Q1AM

7. PERFORMING ORGANIZATION NAME(S) AND ADDRESS(ES)

Air Force Research Laboratory (AFMC)
AFRL/RQRS
1 Ara Drive
Edwards AFB, CA 93524-7013

8. PERFORMING ORGANIZATION REPORT NO.

9. SPONSORING / MONITORING AGENCY NAME(S) AND ADDRESS(ES)

Air Force Research Laboratory (AFMC)
AFRL/RQR
5 Pollux Drive
Edwards AFB, CA 93524-7048

10. SPONSOR/MONITOR'S ACRONYM(S)

11. SPONSOR/MONITOR'S REPORT NUMBER(S)
AFRL-RQ-ED-JA-2015-175

12. DISTRIBUTION / AVAILABILITY STATEMENT
Approved for public release; distribution unlimited

13. SUPPLEMENTARY NOTES
Journal article published in the Journal of Applied Physics, Vol. #118, Issue #13, October 2015
PA Case Number: #15301; Clearance Date: 6/3/2015

14. ABSTRACT
The objective of the present work is the development a tightly coupled magneto-hydrodynamic model for Inductively Coupled Radio-Frequency (RF) Plasmas. Non Local Thermodynamic Equilibrium (NLTE) effects are described based on a hybrid State-to-State (StS) approach. A multi-temperature formulation is used to account for thermal non-equilibrium between translation of heavy-particles and vibration of molecules. Excited electronic states of atoms are instead treated as separate pseudo-species, allowing for non-Boltzmann distributions of their populations. Free-electrons are assumed Maxwellian at their own temperature. The governing equations for the electro-magnetic field and the gas properties (e.g. chemical composition and temperatures) are written as a coupled system of time-dependent conservation laws. Steady-state solutions are obtained by means of an implicit Finite Volume method. The results obtained in both LTE and NLTE conditions over a broad spectrum of operating conditions demonstrate the robustness of the proposed coupled numerical method. The analysis of chemical composition and temperature distributions along the torch radius shows that: (i) the use of the LTE assumption may lead to an inaccurate prediction of the thermo-chemical state of the gas, and (ii) non-equilibrium phenomena play a significant role close the walls, due to the combined effects of Ohmic heating and macroscopic gradients.

15. SUBJECT TERMS
N/A

16. SECURITY CLASSIFICATION OF:			**17. LIMITATION OF ABSTRACT**	**18. NUMBER OF PAGES**	**19a. NAME OF RESPONSIBLE PERSON**
					J-L. Cambier
a. REPORT	**b. ABSTRACT**	**c. THIS PAGE**	SAR	13	**19b. TELEPHONE NO** *(include area code)*
Unclassified	**Unclassified**	**Unclassified**			N/A

Standard Form 298 (Rev. 8-98)
Prescribed by ANSI Std. 239.18

A tightly coupled non-equilibrium magneto-hydrodynamic model for Inductively Coupled RF Plasmas

A. Munafò,[1, a)] S. A. Alfuhaid,[1, b)] J.-L. Cambier,[2, c)] and M. Panesi[1, d)]
[1)] *Department of Aerospace Engineering, University of Illinois at Urbana-Champaign, Talbot Lab., 104 S. Wright St., Urbana, 61801 IL*
[2)] *Edwards Air Force Base Research Lab., 10 E. Saturn Blvd., CA 93524*

(Dated: 7 May 2015)

The objective of the present work is the development a tightly coupled magneto-hydrodynamic model for Inductively Coupled Radio-Frequency (RF) Plasmas. Non Local Thermodynamic Equilibrium (NLTE) effects are described based on a hybrid State-to-State (StS) approach. A multi-temperature formulation is used to account for thermal non-equilibrium between translation of heavy-particles and vibration of molecules. Excited electronic states of atoms are instead treated as separate *pseudo-species*, allowing for non-Boltzmann distributions of their populations. Free-electrons are assumed Maxwellian at their own temperature. The governing equations for the electro-magnetic field and the gas properties (*e.g.* chemical composition and temperatures) are written as a coupled system of time-dependent conservation laws. Steady-state solutions are obtained by means of an implicit Finite Volume method. The results obtained in both LTE and NLTE conditions over a broad spectrum of operating conditions demonstrate the robustness of the proposed coupled numerical method. The analysis of chemical composition and temperature distributions along the torch radius shows that: (i) the use of the LTE assumption may lead to an inaccurate prediction of the thermo-chemical state of the gas, and (ii) non-equilibrium phenomena play a significant role close the walls, due to the combined effects of Ohmic heating and macroscopic gradients.

I. INTRODUCTION

Inductively Coupled Plasma (ICP) torches have wide range of possible applications which include deposition of metal coatings, synthesis of ultra-fine powders, generation of high purity silicon and testing of thermal protection materials for atmospheric entry vehicles.[1,2] In its simplest configuration, an ICP torch consists of a quartz tube surrounded by an inductor coil made of a series of parallel current-carrying rings (see Fig. 1).

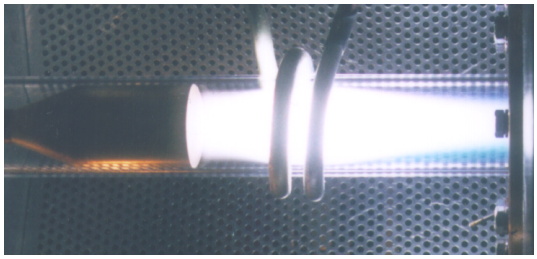

FIG. 1. Example of ICP torch in operating conditions (mini-torch facility; credits von Karman Institute for Fluid Dynamics).

The radio-frequency (RF) currents running through the inductor induce toroidal currents in the gas which is heated thanks to Ohmic dissipation.[2,3] If the energy supplied is large enough, the gas flowing through the torch can undergo ionization, leading to the formation of a plasma.

The physico-chemical modeling of the flow-field and electromagnetic phenomena inside an ICP torch requires, in theory, the coupled solution of the Navier-Stokes and the Maxwell equations. The numerical solution of this coupled system of partial differential equations represents a challenging task, due to the disparity between the flow and the electro-magnetic field time-scales.[4] Since in the modeling of ICP facilities one is not normally interested in resolving electro-magnetic field oscillations,[5] displacement currents can be safely neglected without introducing an appreciable error.[2,6] This leads to a more tractable formulation, as it eliminates the speed of light from the eigenvalues of the governing equations.[4]

The first attempts to model the temperature and electro-magnetic field distributions inside ICP torches were published in the 1960-1970's. Examples are the works of Freeman and Chase,[7] Keefer *et. al.*,[8] and the series of papers by Eckert.[9–12] In most of these references, the torch was approximated as an infinite solenoid and the plasma generated was considered in Local Thermodynamic Equilibrium (LTE) conditions. This reduces the problem to the coupled solution of the energy equation for the gas (known as the *Elenbaas-Heller* equation[7,13]) and an induction equation for the electric field. The induction equation is formally identical to the one describing induction heating of metals.[14,15] The authors use the heat conduction potential (*i.e.* $s = \int \kappa \, dT$), in place of the temperature T, as thermodynamic variable. This choice allows one to hide the non-linearity of the gas (total) thermal conductivity κ and can partially alle-

[a)] Electronic mail: munafo@illinois.edu
[b)] Electronic mail: alfuhai2@illinois.edu
[c)] Electronic mail: jean_luc.cambier@us.af.mil
[d)] Electronic mail: mpanesi@illinois.edu

viate numerical instabilities that may arise when solving the discretized set of equations by means of an iterative procedure. As recognized by Pridmore and Brown,[16] the use of the heat conduction potential becomes less effective for molecular gases (*e.g.* air and nitrogen mixtures). The major developments achieved in the field of Computational Fluid Dynamics (CFD) during the 1970-1980's, led to the possibility of solving the ICP magneto-hydrodynamic equations in multi-dimensional configurations. Examples are given in the papers by Boulos,[17] Mostaghimi, Proulx Bouos and co-workers,[18–23] Kolesnikov and co-workers,[24–30] Chen and Pfender,[31] van den Abeele and Degrez[32], and more recently Panesi *et. al.*[33] and Morsli and Proulx.[34] In these works, numerical solutions are obtained using an *explicit coupling* approach, by solving independently the flow and the electric field governing equations, and updating coupling terms after each iteration. As observed by van den Abeele and Degrez,[32] the *explicit coupling* approach prevents the use of Newton's method during the first iterations and requires to resort to more conservative iterative techniques (*e.g* Picard's method[32]) at the beginning of the simulation. Convergence issues with Newton's method may also arise when solving the flow governing equations in time-dependent form. This is especially true when the current intensity in the inductor is updated to match the imposed value of the power dissipated in the plasma. The cause of the instability is most probably due to the *lagged update* of the Joule heating term in the energy equation, which is quadratic in the electric field amplitude.[17,31,32]

Most of the simulations available in the literature assume that the plasma in the torch is in LTE conditions.[17–19,31–33,35] This assumption is often justified by saying that, for the pressure values at which ICP facilities are operated (*e.g.* $\approx 10^4$ Pa and above), the collisional rate among the gas particles are sufficiently large to maintain local equilibrium. A second, and more practical reason, is the significant stiffness and CPU time reduction compared to Non-LTE (NLTE) situations. Moreover, in LTE conditions, the gas thermodynamic and transport properties are only function of two independent state variables[36] (*e.g.* pressure and temperature). Hence, they can be easily tabulated to further reduce the computational time. Simulations performed by Mostaghimi *et al.*[20,22] and by Zhang *et al.*[37] (in Argon and air plasmas, respectively) have shown, however, that the use of the LTE assumption may not always hold.

An accurate modeling of NLTE effects in ICP plasmas can be achieved by means of State-to-State (StS) models.[38–50] These treat each internal energy state as a separate *pseudo species*, thus allowing for non-Boltzmann distributions. Rate coefficients are usually obtained through quantum chemistry calculations[51–56] or through phenomenological models providing a simplified description of the kinetic process under investigation.[57,58] State-to-State models provide a superior description compared to conventional multi-temperature models, which are based on Maxwell-Boltzmann distributions.[59–62] However, due to the large number of governing equations to be solved, their application to multi-dimensional problems can become computationally demanding.[63–67]

The purpose of the present paper is development of a tightly coupled non-equilibrium model for ICP RF plasmas. To alleviate the possible occurrence of numerical instabilities, typical of an *explicit coupling* approach, the following steps are taken: (i) the flow and the induced electric field governing equations are solved in a fully coupled fashion, and (ii) steady-state solutions are obtained by means of a time-marching approach (as often done in CFD applications[68]). The governing equations are discretized in space by using the Finite Volume method. Time-integration is then performed by means of a fully implicit method. As it is shown in the paper, the time-dependent formulation introduces a *local relaxation* in the set of space-discretized equations, which enhances convergence significantly. The computational ICP framework developed in this work allows for the use of both LTE and NLTE physico-chemical models. Non-LTE effects are described based on a hybrid StS model. A multi-temperature (MT) formulation is used to account for thermal non-equilibrium between translation of heavy-particles and vibration of molecules. Excited electronic states of atoms are instead treated as separate *pseudo-species*. Free-electrons are assumed Maxwellian at their own temperature.

The paper is organized as follows. Section II describes the physical model. The numerical method for solving the governing equations is given in Sec. III. Computational results are presented in Sec. IV. Conclusions are discussed in Sec. V.

II. PHYSICAL MODELING

This section describes the physical model developed for the investigation of non-equilibrium effects in ICP RF plasmas. The non-equilibrium model for the ICP torch is built based on the torch geometry displayed in Fig. 2. To make the problem tractable, the following assumptions are introduced:

(i) Constant pressure and no *macroscopic streaming*,

(ii) Charge neutrality and no displacement current,

(iii) Steady-state conditions for gas quantities (*i.e.* $\partial()/\partial t = 0$),

(iv) No gradients along the axial and circumferential directions (*i.e.* $\partial()/\partial z = 0$, $\partial()/\partial \phi = 0$).

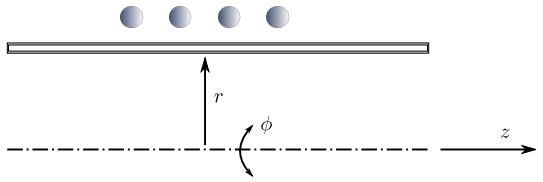

FIG. 2. Torch geometry and adopted reference frame.

A. Electro-magnetic field

The electromagnetic field inside the ICP torch is described by the Maxwell equations:

$$\nabla \cdot \mathbf{E} = \frac{\rho^{\mathrm{c}}}{\epsilon_0}, \quad \nabla \cdot \mathbf{B} = 0, \tag{1}$$

$$\nabla \times \mathbf{E} = -\frac{\partial \mathbf{B}}{\partial t}, \quad \nabla \times \mathbf{B} = \mu_0 \mathbf{J} + \mu_0 \epsilon_0 \frac{\partial \mathbf{E}}{\partial t}, \tag{2}$$

where quantities $\mathbf{E}$ and $\mathbf{B}$ are the electric and magnetic fields, respectively. Quantity ρ^{c} stands for the charge density. The current density $\mathbf{J}$ is assumed to obey Ohm's law $\mathbf{J} = \sigma_{\mathrm{e}}\mathbf{E}$, with σ_{e} being the electrical conductivity. Quantities ϵ_0 and μ_0 are the vacuum permittivity and magnetic permeability, respectively. The application of the simplifying assumptions just introduced to the Maxwell equations (1)-(2) leads to the induction equation for the induced toroidal electric field:

$$\frac{\partial}{\partial r}\left(\frac{1}{r}\frac{\partial r E_\phi}{\partial r}\right) = -\mu_0 \sigma_{\mathrm{e}} \frac{\partial E_\phi}{\partial t}. \tag{3}$$

Since the induced eddy currents which are responsible for the heating of the gas are induced by a primary current whose intensity varies sinusoidally in time, it seems natural to seek for a monochromatic wave solution, $E_\phi = E\exp(\imath\omega t)$, where $\omega = 2\pi f$ (with f being the frequency of the primary current). To account for the possible phase difference between the electric and magnetic fields, the amplitude E is taken complex, $E = E_{\mathrm{re}} + \imath E_{\mathrm{im}}$. The substitution of $E\exp(\imath\omega t)$ in Eq. (3) leads to:

$$0 \times \frac{\partial r \mathbf{U}_{\mathrm{em}}}{\partial t} + \frac{\partial r \mathbf{F}_{\mathrm{em}}}{\partial r} = r\mathbf{S}_{\mathrm{em}}. \tag{4}$$

The electromagnetic (em) conservative variable, flux and source term vectors are:

$$\mathbf{U}_{\mathrm{em}} = \left[\begin{array}{cc} E_{\mathrm{re}} & E_{\mathrm{im}} \end{array}\right]^{\mathrm{T}}, \tag{5}$$

$$\mathbf{F}_{\mathrm{em}} = \left[\begin{array}{cc} \dfrac{\partial E_{\mathrm{re}}}{\partial r} & \dfrac{\partial E_{\mathrm{im}}}{\partial r} \end{array}\right]^{\mathrm{T}}, \tag{6}$$

$$\mathbf{S}_{\mathrm{em}} = \left[\begin{array}{cc} \dfrac{E_{\mathrm{re}}}{r^2} + \omega\mu_0\sigma_{\mathrm{e}}E_{\mathrm{im}} & \dfrac{E_{\mathrm{im}}}{r^2} - \omega\mu_0\sigma_{\mathrm{e}}E_{\mathrm{re}} \end{array}\right]^{\mathrm{T}}. \tag{7}$$

Equation (4) must be supplemented with boundary conditions at the axis ($r = 0$) and at the torch wall ($r = R$, with R being the torch radius). On the axis, due to symmetry, both components of the electric field must vanish:

$$E_{\mathrm{re}} = 0, \quad E_{\mathrm{im}} = 0, \quad \text{at } r = 0. \tag{8}$$

The boundary condition at the torch wall is obtained as follows. The amplitudes of the toroidal electric field and the axial magnetic field are linked via:[6]

$$\frac{1}{r}\frac{\partial r E}{\partial r} = -\imath\omega B, \tag{9}$$

where the amplitude B is taken complex. Immediately outside the wall the magnetic field must be real and, since there is no plasma outside the tube, its value can only depend on the ICP operating conditions and characteristics. If the torch is long enough, the magnetic field at the torch wall can be approximated with the expression for an infinite solenoid, $B = \mu_0 N I_{\mathrm{c}}$, where quantities N and I_{c} are the number of turns per unit-length and the amplitude of the primary current. The evaluation of Eq. (9) at the torch wall and the use of the relation $B = \mu_0 N I_{\mathrm{c}}$ gives the wall boundary condition for the induced electric field:

$$\frac{1}{r}\frac{\partial r E_{\mathrm{re}}}{\partial r} = 0, \quad \frac{1}{r}\frac{\partial r E_{\mathrm{im}}}{\partial r} = -\omega\mu_0 N I_{\mathrm{c}}, \text{ at } r = R. \tag{10}$$

B. Hydro-dynamics

The gas contained in the torch is made of electrons, atoms and molecules. Charged particles comprise electrons and positively singly charged ions. The set $\mathcal{S}$ stores the chemical components, and the heavy-particles are stored in the set $\mathcal{S}_{\mathrm{h}}$. The atomic and molecular components are stored in the sets $\mathcal{S}_{\mathrm{a}}$ and $\mathcal{S}_{\mathrm{m}}$, respectively. The previously introduced sets satisfy the relations $\mathcal{S}_{\mathrm{h}} = \mathcal{S}_{\mathrm{a}} \cup \mathcal{S}_{\mathrm{m}}$ and $\mathcal{S} = \{\mathrm{e}^-\} \cup \mathcal{S}_{\mathrm{h}}$, where the symbol e^- indicates the free-electrons. The electronic levels of the heavy components are stored in sets $\mathcal{I}_s^{\mathrm{el}}$ (with $s \in \mathcal{S}_{\mathrm{h}}$) and are treated as separate *pseudo species* based on a StS approach.[69] The notation s_i is used to denote the i-th electronic level of the heavy component $s \in \mathcal{S}_{\mathrm{h}}$, with the related degeneracy and energy being $g_{s_i}^{\mathrm{el}}$ and $E_{s_i}^{\mathrm{el}}$, respectively. A multi-temperature model is instead used for vibration of molecules and translation of free-electrons (with the related temperatures being T_{v} and T_{e}, respectively).[60] Rotational non-equilibrium effects are disregarded.

Thermodynamic properties

The gas pressure is computed as $p = p_{\mathrm{e}} + p_{\mathrm{h}}$, where the symbol $\mathrm{k_B}$ stands for Boltzmann's constant. The partial pressures of free-electrons and heavy-particles are, respectively, $p_{\mathrm{e}} = n_{\mathrm{e}}\mathrm{k_B}T_{\mathrm{e}}$ and $p_{\mathrm{h}} = n_{\mathrm{h}}\mathrm{k_B}T$, where quantities n_{e} and n_{h} denote, respectively, the related the number densities (with $n_{\mathrm{h}} = \sum_{s\in\mathrm{S}_h} n_s$ and $n_s = \sum_{i\in\mathcal{I}_s^{\mathrm{el}}} n_{s_i}$). The gas total, rotational, vibrational and free-electron energy densities are:

$$\rho e = \frac{3}{2}p + \rho e_{\mathrm{r}} + \rho e_{\mathrm{v}} + \sum_{s\in\mathcal{S}_{\mathrm{h}}}\sum_{i\in\mathcal{I}_s^{\mathrm{el}}} n_{s_i}(E_{s_i}^{\mathrm{el}} + \Delta E_s^{\mathrm{f}}) \tag{11}$$

$$\rho e_{\rm r} = \sum_{s\in\mathcal{S}_{\rm m}} n_s \tilde{E}^{\rm r}_s(T),\ \rho e_{\rm v} = \sum_{s\in\mathcal{S}_{\rm m}} n_s \tilde{E}^{\rm v}_s(T_{\rm v}),\ \rho e_{\rm e} = \frac{3}{2} p_{\rm e}. \tag{12}$$

Quantity $\Delta E^{\rm f}_s$ stands for the formation energy (per particle) of the heavy component $s \in \mathcal{S}_{\rm h}$. The average particle rotational and vibrational energies ($\tilde{E}^{\rm r}_s$ and $\tilde{E}^{\rm v}_s$, $s \in \mathcal{S}_{\rm m}$,respectively) are computed, respectively, according to the rigid-rotor and harmonic-oscillator models[70]. Thermodynamic data used in this work are taken from Gurvich tables[71] (with the exception of the spectroscopic data for the electronic levels taken from Ref. 43).

Chemical-kinetics

The NLTE kinetic mechanism for ICP RF plasmas developed in this work accounts for:

(i) Excitation by electron impact,

(ii) Ionization by electron impact,

(iii) Dissociation by electron impact,

(iv) Dissociation by heavy-particle impact,

(v) Associative ionization.

The endothermic rate coefficients for electron induced processes and associative ionization reactions are taken from the ABBA StS model.[43–46] Those for dissociation by heavy-particle impact are taken from the work of Park.[60] Reverse rate coefficients are obtained based on microreversibility.[72,73]

The mass production terms for free-electrons and heavy-particles are computed based on the zeroth-order reaction rate theory.[72,73] In what follows, the latter quantities are indicated with the notation $\omega_{\rm e}$ and ω_{s_i}, respectively

The energy transfer terms for the gas vibrational energy account for (i) vibrational-translational (vt) energy exchange in molecule heavy-particle collisions, (ii) vibrational-electron (ve) energy exchange in molecule electron collisions, and (iii) the creation/destruction of vibrational energy in chemical reactions (cv). The first two energy transfer terms (indicated in what follows with $\Omega_{\rm vt}$ and $\Omega_{\rm ve}$, respectively) are evaluated based on a Landau-Teller model,[74] while the chemistry-vibration coupling term ($\Omega_{\rm cv}$) is computed by using the non-preferential dissociation model of Candler.[75] The relaxation times for vt energy transfer are computed by means of the modified formula of Millikan and White proposed by Park.[60] The energy transfer in molecule-electron inelastic collisions is considered only for N_2. The corresponding relaxation time is taken from the work of Bourdon.[76] The energy transfer terms for the free-electron gas account for energy exchange undergone by free-electrons in (i) elastic collisions with heavy-particles ($\Omega_{\rm el}$), (ii) inelastic electron induced excitation, ionization and dissociation processes ($\Omega_{\rm in}$) and (iii) Joule heating ($\Omega_{\rm j}$). The expressions for the first two can be found in Refs. 44–46. The (time-averaged) Joule heating source term is obtained by averaging over a period the instantaneous Joule heating power and reads $\Omega_{\rm j} = \sigma_{\rm e}(E^2_{\rm re} + E^2_{\rm im})/2$.[31,32]

Transport properties and fluxes

Transport phenomena are treated based on the results of the Chapman-Enskog method for the Boltzmann equation[77] under the assumption that: (i) inelastic and reactive collisions have a no effect on the transport properties and fluxes and (ii) the collision cross-sections for elastic scattering do not depend on the internal quantum states.

The translational component of thermal conductivity is $\lambda_{\rm t} = \sum_{s\in\mathcal{S}_{\rm h}} \alpha^\lambda_s X_s$, where the mole fractions of the heavy components are $X_s = n_s {\rm k_B} T/p$ ($s \in \mathcal{S}_{\rm h}$). The coefficients α^λ_s are solution of the linear (symmetric) transport system for the translational thermal conductivity (see, for instance, Ref. 72 for the details). The contributions of the gas rotational and vibrational degrees of freedom to the thermal conductivity ($\lambda_{\rm r}$ and $\lambda_{\rm v}$, respectively) are taken into account by means of the generalized Eucken's correction.[72] The thermal and electrical conductivity of the electron gas are:[78,79]

$$\lambda_{\rm e} = \frac{75}{8}{\rm k_B}\sqrt{\frac{2\pi {\rm k_B} T_{\rm e}}{m_{\rm e}}}\frac{X_{\rm e}\Lambda^{22}_{\rm ee}}{\Lambda^{11}_{\rm ee}\Lambda^{22}_{\rm ee} - (\Lambda^{12}_{\rm ee})^2}, \tag{13}$$

$$\sigma_{\rm e} = \frac{3}{2}\frac{{\rm e}^2}{{\rm k_B}}\sqrt{\frac{2\pi {\rm k_B}}{m_{\rm e} T_{\rm e}}}\frac{X_{\rm e}\Lambda^{11}_{\rm ee}}{\Lambda^{00}_{\rm ee}\Lambda^{11}_{\rm ee} - (\Lambda^{10}_{\rm ee})^2}, \tag{14}$$

where the mole fraction of free-electrons is $X_{\rm e} = n_{\rm e}{\rm k_B}T_{\rm e}/p$ and ${\rm e} = 1.602\times10^{-19}$ C is the electron charge. Quantities $\Lambda^{ij}_{\rm ee}$ denote the Devoto collision integrals.[78]

The mass diffusion fluxes are found by solving the Stefan-Maxwell equations under the constraints of global mass conservation and ambipolar diffusion.[78–81] The diffusion driving forces include only mole fraction gradients. In view of the assumed independence of the elastic collision cross-section on the internal quantum states, the Stefan-Maxwell equations are solved for the diffusion fluxes of chemical components ($J_{\rm e}$ and J_s, $s \in \mathcal{S}_{\rm h}$, respectively). The mass diffusion fluxes for the internal levels (J_{s_i}), are then found as shown in Ref. 6. The gas total, rotational, vibrational and free-electron heat flux are:

$$q = \sum_{s\in\mathcal{S}_{\rm h}}\sum_{i\in\mathcal{I}^{\rm el}_s}\left(\frac{5}{2}{\rm k_B}T + E^{\rm el}_{s_i} + \Delta E^{\rm f}_s\right)\frac{J_{s_i}}{m_s} - \lambda_{\rm t}\frac{\partial T}{\partial r} + q_{\rm r} + q_{\rm v} + q_{\rm e}, \tag{15}$$

$$q_{\rm r} = \sum_{s\in\mathcal{S}_{\rm m}} \tilde{E}^{\rm r}_s(T)\frac{J_s}{m_s} - \lambda_{\rm r}\frac{\partial T}{\partial r}, \tag{16}$$

$$q_{\rm v} = \sum_{s\in\mathcal{S}_{\rm m}} \tilde{E}^{\rm v}_s(T_{\rm v})\frac{J_s}{m_s} - \lambda_{\rm v}\frac{\partial T_{\rm v}}{\partial r}, \tag{17}$$

$$q_{\rm e} = \left(\frac{5}{2}{\rm k_B}T_{\rm e}\right)\frac{J_{\rm e}}{m_{\rm e}} - \lambda_{\rm e}\frac{\partial T_{\rm e}}{\partial r}. \tag{18}$$

Governing equations

The governing equations for the gas chemical composition and temperature distribution in the ICP torch are:

$$\frac{\partial r\mathbf{U}_\mathrm{g}}{\partial t}+\frac{\partial r\mathbf{F}_\mathrm{g}}{\partial r}=r\mathbf{S}_\mathrm{g}. \tag{19}$$

The gas (g) conservative variable, flux and source term vectors are:

$$\mathbf{U}_\mathrm{g}=\left[\begin{array}{ccccc}\rho_\mathrm{e} & \rho_{s_i} & \rho e & \rho e_\mathrm{v} & \rho e_\mathrm{e}\end{array}\right]^\mathrm{T}, \tag{20}$$

$$\mathbf{F}_\mathrm{g}=\left[\begin{array}{ccccc}J_\mathrm{e} & J_{s_i} & q & q_\mathrm{v} & q_\mathrm{e}\end{array}\right]^\mathrm{T}, \tag{21}$$

$$\mathbf{S}_\mathrm{g}=\left[\begin{array}{ccccc}\omega_\mathrm{e} & \omega_{s_i} & \Omega_\mathrm{j} & \Omega_\mathrm{v} & \Omega_\mathrm{e}\end{array}\right]^\mathrm{T}, \tag{22}$$

$i\in\mathcal{I}_s^\mathrm{el}$, $s\in\mathcal{S}_\mathrm{h}$, with $\Omega_\mathrm{v}=\Omega_\mathrm{vt}+\Omega_\mathrm{ve}+\Omega_\mathrm{cv}$ and $\Omega_\mathrm{e}=\Omega_\mathrm{el}+\Omega_\mathrm{in}+\Omega_\mathrm{j}$.

The boundary conditions used for solving Eq. (19) are a symmetry boundary condition at the axis and an isothermal non-catalytic boundary condition at the torch wall. Following the work of Mostaghimi *et al.*,[20,22] an adiabatic wall boundary condition is used for the vibrational and free-electron temperatures.

III. NUMERICAL METHOD

The governing equations for the gas and the electromagnetic fields are strongly coupled due to the presence of the Joule heating term in Eq. (22) and the electrical conductivity in Eq. (7). This suggests to adopt a fully coupled approach by casting Eqs. (4) and (19):

$$\frac{\partial r\mathbf{\Gamma}\mathbf{U}}{\partial t}+\frac{\partial r\mathbf{F}}{\partial r}=r\mathbf{S}, \tag{23}$$

where the conservative variable, flux and source term vectors are now $\mathbf{U}=(\mathbf{U}_\mathrm{g},\,\mathbf{U}_\mathrm{em})$, $\mathbf{F}=(\mathbf{F}_\mathrm{g},\,\mathbf{F}_\mathrm{em})$ and $\mathbf{S}=(\mathbf{S}_\mathrm{g},\,\mathbf{S}_\mathrm{em})$, respectively. The matrix $\mathbf{\Gamma}$ in Eq. (23) reads:

$$\mathbf{\Gamma}=\begin{pmatrix}\mathbf{I}_{(\mathrm{ns}+\mathrm{nt})\times(\mathrm{ns}+\mathrm{nt})} & \mathbf{0}_{(\mathrm{ns}+\mathrm{nt})\times 2}\\ \mathbf{0}_{2\times(\mathrm{ns}+\mathrm{nt})} & \mathbf{0}_{2\times 2}\end{pmatrix}, \tag{24}$$

where quantities $\mathbf{I}$ and $\mathbf{0}$ are, respectively, the identity and null matrices. Their number of rows and columns are indicated by the first and second lower-scripts, respectively. The symbols ns and nt denote, respectively, the number of species and temperatures.

Spatial discretization

The application of the Finite Volume method to Eq. (23) leads to the following ODE governing the time-evolution of the conservative variables of cell j:[68]

$$\mathbf{\Gamma}\frac{\partial\mathbf{U}_j}{\partial t}r_j\Delta r_j=-\mathbf{Res}_j. \tag{25}$$

The right-hand-side residual reads:

$$\mathbf{Res}_j=r_{j+\frac{1}{2}}\mathbf{F}_{j+\frac{1}{2}}-r_{j-\frac{1}{2}}\mathbf{F}_{j-\frac{1}{2}}-\mathbf{S}_j\,r_j\,\Delta r_j, \tag{26}$$

where the cell volume (length) and its centroid location are computed as $\Delta r_j=r_{j+1/2}-r_{j-1/2}$ and $r_j=(r_{j+1/2}+r_{j-1/2})/2$, respectively. The evaluation of the diffusive flux $\mathbf{F}_{j+1/2}$ is performed by approximating the values and the gradients of a given quantity p (*e.g.* temperatures and electric field components) by means of an arithmetic average and a second order central finite difference, respectively. To facilitate the implementation of the constant pressure constraint, the solution update is performed on primitive variables ($\mathbf{P}$) consisting of mass fractions, temperatures and electric field components, $\mathbf{P}=(y_\mathrm{e},y_{s_i},\,T,\,T_\mathrm{v},\,T_\mathrm{e},\,E_\mathrm{re},\,E_\mathrm{im})$:

$$\mathbf{\Gamma}\mathbf{T}_j\frac{\partial\mathbf{P}_j}{\partial t}r_j\Delta r_c=-\mathbf{Res}_j. \tag{27}$$

The transformation matrix $\mathbf{T}$ can be obtained from the time-derivative of the conservative variables ($\partial\mathbf{U}/\partial t$) by exploiting the global continuity equation, $\partial\rho/\partial t=0$.

A. Temporal discretization

Equation (27) is integrated in time by means of the backward Euler method:[68]

$$\mathbf{\Gamma}\mathbf{T}_j^n\frac{\delta\mathbf{P}_j^n}{\Delta t_j}r_j\Delta r_j=-\mathbf{Res}_j^{n+1}, \tag{28}$$

where $\delta\mathbf{P}_j^n=\mathbf{P}_j^{n+1}-\mathbf{P}_j^n$. The local time-step Δt is computed based on the von Neumann number (ξ) as $\Delta t=\xi/(2\rho^\mathrm{d})$, where quantity ρ^d stands for the spectral radius of the diffusive flux Jacobian matrix $\partial\mathbf{F}/\partial\mathbf{U}$.[68] To advance the solution from the time-level n to the time-level $n+1$, Eq. (28) is linearized around the time-level n. The outcome of the linearization is a block-tridiagonal algebraic system to be solved at each time-step:[68,82]

$$\mathbf{L}_j^n\,\delta\mathbf{P}_{j-1}^n+\mathbf{C}_j^n\,\delta\mathbf{P}_j^n+\mathbf{R}_j^n\,\delta\mathbf{P}_{j+1}^n=-\mathbf{Res}_j^n, \tag{29}$$

where the left, right and central block matrices are:

$$\mathbf{L}_j=\frac{2\,r_{j-1/2}}{\Delta r_j+\Delta r_{j-1}}\mathbf{A}_{j-\frac{1}{2}}, \tag{30}$$

$$\mathbf{R}_j=\frac{2\,r_{j+1/2}}{\Delta r_j+\Delta r_{j+1}}\mathbf{A}_{j+\frac{1}{2}}, \tag{31}$$

$$\mathbf{C}_j=\left[\frac{\mathbf{\Gamma}\mathbf{T}_j}{\Delta t_j}-\left(\frac{\partial\mathbf{S}}{\partial\mathbf{P}}\right)_j\right]r_j\Delta r_j-(\mathbf{L}_j+\mathbf{R}_j), \tag{32}$$

where quantity $\mathbf{A}$ stands for the (primitive) diffusive flux Jacobian matrix, $\mathbf{A}=\partial\mathbf{F}/\partial\mathbf{P}$. The block-tridiagonal system (29) is solved by means of Thomas' algorithm[68] and the solution updated at the next time-level, $\mathbf{P}_j^{n+1}=\mathbf{P}_j^n+\delta\mathbf{P}_j^n$. This process is continued until steady-state is reached.

Notice that the discretized time derivative in Eq. (32) plays the role of a *relaxation term*. Setting this term to zero (*i.e.* infinite time-step) is equivalent to solve the steady-state form of the governing equations (23) by means of Newton's method. Preliminary calculations performed in LTE conditions indicated that this strategy can easily lead to numerical instability problems in the initial transient of the simulation.

IV. APPLICATIONS

The gas contained in torch consists of molecular nitrogen and the related dissociation and ionization products, $\mathcal{S} = \{e^-, N, N_2, N_2^+, N^+\}$. Simulations have been performed by means of the ABBA StS model[43–46] and the MT model developed by Park.[60]

The torch radius, the number of coils per unit-length and the wall temperature are set to 0.08 m, 50, and 350 K, respectively. The current intensity of the primary circuit is found from the solution by imposing that the dissipated power (per unit-length) in the plasma:

$$P = 2\pi \int_0^R \Omega_j \, r \, dr, \tag{33}$$

is equal to a fixed value P_0. To match the condition $P = P_0$ at steady-state, the current intensity is multiplied by the scaling factor $\gamma = \sqrt{P_0/P}$ after updating the solution at the new time-step. This approach was originally introduced by Boulos[17] in the 1970's, and it has been used since then by other investigators.[18,31–33,37] In the present work, no scaling is applied to the electric field (as opposed to *explicit coupling* methods[32]), due to the use of a fully coupled formulation.

In order to assess the influence of the ICP operating conditions on non-equilibrium effects, different values of pressure, frequency of the primary circuit and dissipated power have been adopted (see Table I).

TABLE I. Adopted values for the pressure, frequency of the primary circuit and dissipated power (per unit-length) in the plasma.

Quantity	Units	Values
Pressure (p)	Pa	3000, 5000 and 10 000
Frequency (f)	MHz	0.1, 0.5, 1 and 2.5
Dissipated power (P_0)	MW/m	0.2, 0.3, 0.35 and 0.4

A. Performance of the coupled numerical formulation

The coupled numerical method developed in Sect. III has been applied over a wide spectrum of operating conditions (given in Table I) in both LTE and NLTE conditions. In all cases treated in this work, no need arose for the use of techniques to cope with numerical instabilities such as under-relaxation factors, conservative iterative strategies (*e.g.* Picard's method) or choice of a *smart* initial guess for the solution.

To demonstrate in practice the robustness and the effectiveness of the proposed computational method, a MT NLTE simulation has been chosen as working example. The operating conditions are: $p = 10\,000$ Pa, $f = 0.5$ MHz and $P_0 = 0.35$ MW/m. For the sake of simplicity, an isothermal wall boundary conditions has been used for all temperatures. The solution has been initialized with a uniform equilibrium distribution at 7500 K, with both the real and imaginary electric field components set to 0.1 V/m. The initial value of the current intensity was 250 A.

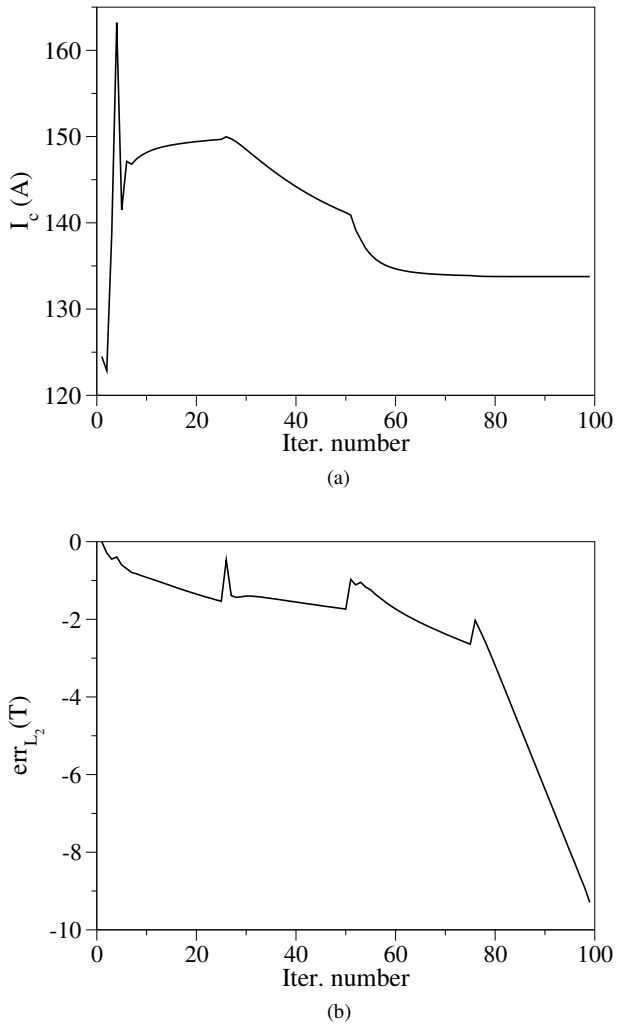

FIG. 3. Time-history of (a) current intensity and (b) normalized L_2 norm of the relative error on the translational-rotational temperature for the MT NLTE model ($p = 10\,000$ Pa, $f = 0.5$ MHz, $P_0 = 0.35$ MW/m; isothermal boundary condition for all temperatures).

In the early stages of the numerical simulation, strong gradients in temperature and chemical composition form in correspondence of the wall, due to the isothermal

boundary condition imposed. Despite the challenges imposed by the problem, the initial value of the von Neuman number was set to to 1×10^5, and increased interactively (every 25 iterations) up to 5×10^8. Such large values were possible due to the adoption of a fully implicit time-integration method. Figure 3 shows the time-history of the current intensity and the L_2 norm of the relative error on the translational-rotational temperature:

$$\mathrm{err}^n_{L_2}(T) = \sqrt{\frac{1}{\mathrm{nc}} \sum_{j=1}^{\mathrm{nc}} (\delta T^n_j)^2}, \tag{34}$$

where quantity nc denotes the number of cells, and $\delta T^n_j = T^{n+1}_j - T^n_j$. A converged solution is achieved in less than 100 iterations (see Fig. 3(b)), with a reduction of more than nine orders of magnitude in the relative error for the temperature. In practice, the solution is already converged after 80 iterations, as can be observed from the current intensity time-history (see Fig. 3(a)).

Figure 4 shows the temperature distribution along the torch radius. Due to the efficient energy exchange in N_2-e^- interactions,[60,76,83] the vibrational and free-electron temperature profiles are essentially indistinguishable. This feature has been observed in all NLTE simulations performed. This is the reason for the use of the notation T_{ve} in Fig. 4 (and also in what follows).

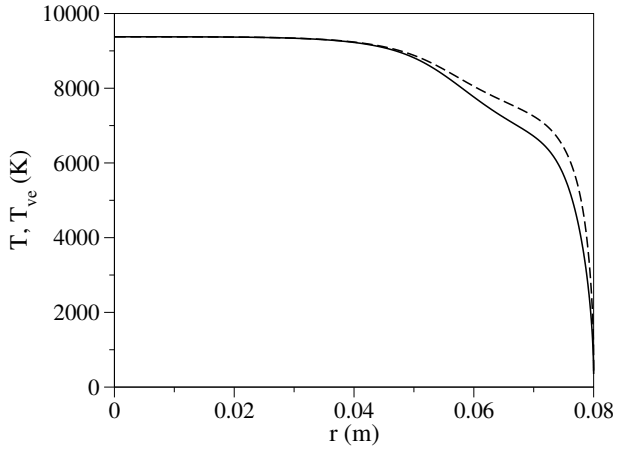

FIG. 4. MT NLTE temperature distribution ($p = 10\,000$ Pa, $f = 0.5$ MHz, $P_0 = 0.35$ MW/m; unbroken line T, dashed-line T_{ve}; isothermal boundary condition for all temperatures).

B. Assessment of non-equilibrium effects

Before discussing in detail NLTE effects, LTE simulations have been performed and compared with the MT NLTE results to assess the extent of the departure from equilibrium. The pressure is set to 10000Pa as, for this relatively high value, LTE conditions are often assumed.[6] The frequency and the dissipated power are 0.5 MHz and 0.35 MW/m, respectively.

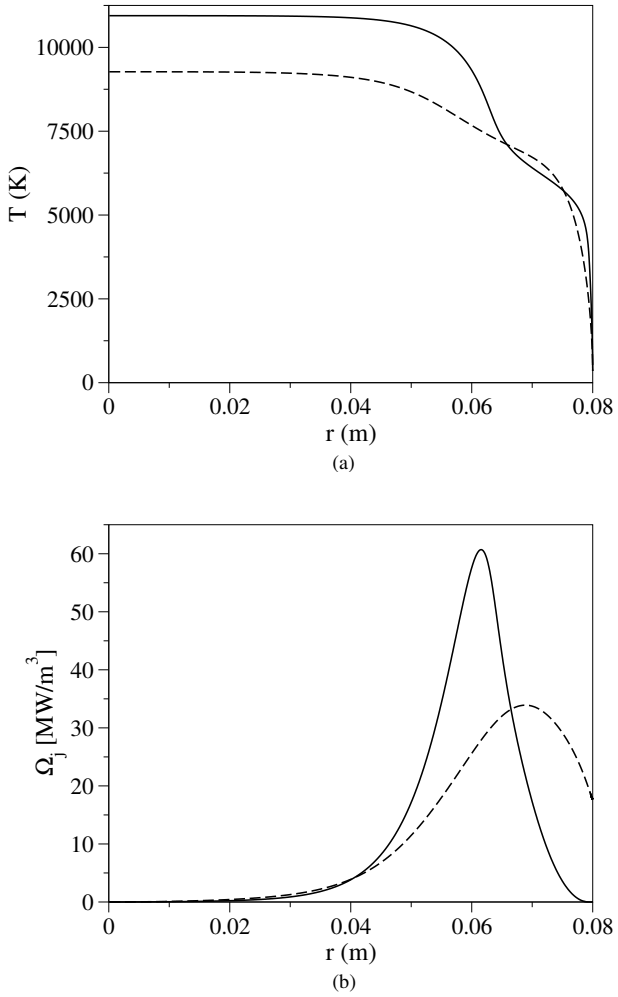

FIG. 5. Comparison between the LTE and the MT NLTE temperature (a) and Joule heating (b) distributions ($p = 10\,000$ Pa, $f = 0.5$ MHz, $P_0 = 0.35$ MW/m; unbroken line LTE, dashed line NLTE).

Figure 5 compares the LTE and NLTE translational-rotational temperature and Joule heating distributions. Close to the wall, the curvature of the LTE temperature distribution changes sign. This is a consequence of the non-monotone behavior of the equilibrium total thermal conductivity of the working gas (nitrogen). The same trend is also found for the MT solution, though less pronounced. The MT model predicts that the gas is in thermal equilibrium close to the axis (see Fig. 4). In both the LTE and NLTE simulations, the temperature is maximum on the axis, due to the absence of radiative losses in the plasma.[9,10] Overall, the LTE solution predicts higher temperature values, with the difference being maximum on the axis. This is a general trend observed in all the simulations performed in this work (and also in the multi-dimensional results obtained by other investigators in Refs. 6 and 37). In NLTE conditions, the temperature is lower because the plasma is heated over a wider region compared to LTE conditions. This is confirmed by the

Joule heating distribution shown in Fig. 5(c). Analogous conclusions can be drawn when comparing with the StS NLTE model adopted in this work.

The results in Fig. 5 demonstrate that, even at relatively high pressures, the LTE assumption can lead to a severe overestimation of the gas temperature and, in general, to an inaccurate prediction of the thermo-chemical state of the gas. This is further confirmed by the comparison for the mole fractions given in Fig. 6. It is worth recalling that in the present work, the effects of macroscopic flows (which enhance non-equilibrium) are neglected.

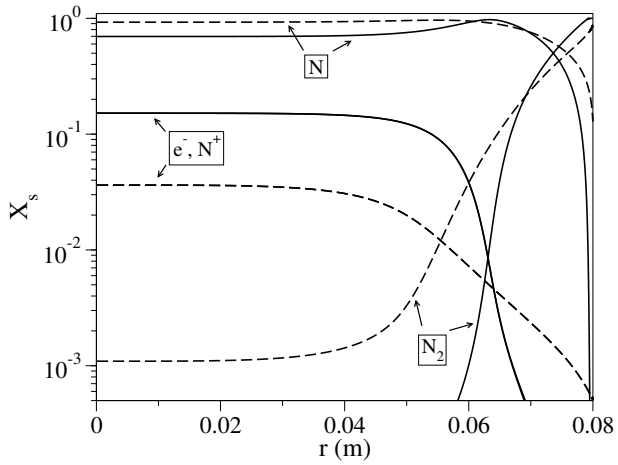

FIG. 6. Comparison between the LTE and the MT NLTE mole fraction distributions ($p = 10\,000$ Pa, $f = 0.5$ MHz, $P_0 = 0.35$ MW/m; unbroken line LTE, dashed line NLTE). Due to the low concentration of N_2^+ (not shown), the mole fractions of e^- and N^+ are essentially indistinguishable in both LTE and NLTE conditions.

C. Influence of frequency and power on non-equilibrium

In order to assess the influence of operating conditions on non-equilibrium phenomena, it was decided to perform a parametric study on the frequency of the primary circuit and the power dissipated in the plasma. Figures 7-8 show the results of this investigation for the MT NLTE model at $p = 5000$ Pa. Increasing the frequency (Fig. 7) has the effect of narrowing the extent of the *skin-depth*, which is the zone over which most of the power is dissipated by Ohmic heating. This can be seen from the relation for the *skin-depth*[14,15], $\delta = (\sigma_e \pi \mu_0 f)^{-1/2}$. The reduction of the *skin-depth* induces sharper gradients close to the wall, thereby enhancing non-equilibrium. These findings are in accordance with the observations reported by Mostaghimi *et al.*[22] for NLTE Argon plasmas. The increase of the dissipated power (Fig. 8) has an opposite effect. As can be observed from the results, higher power levels favor the establishment of thermal equilibrium conditions.

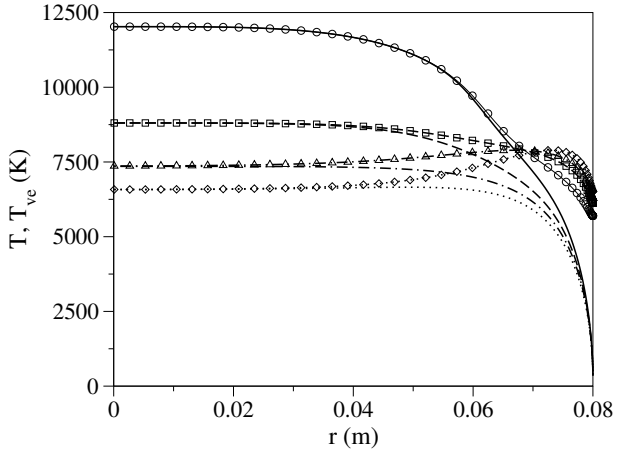

FIG. 7. MT NLTE temperature distributions for different values of the frequency of the primary circuit: unbroken line $f = 0.1$ MHz, dashed line $f = 0.5$ MHz, dotted-dashed line $f = 1$ MHz, dotted line $f = 2.5$ MHz ($p = 5000$ Pa, $P_0 = 0.35$ MW/m; unbroken line T, line with symbols T_{ve}).

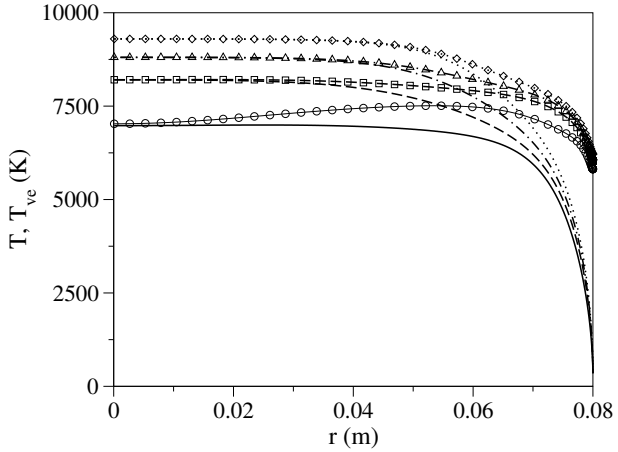

FIG. 8. MT NLTE temperature distributions for different values of the dissipated power (per unit-length) in the plasma: unbroken line $P_0 = 0.2$ MW/m, dashed line $P_0 = 0.3$ MW/m, dotted-dashed line $P_0 = 0.35$ MW/m, dotted line $P_0 = 0.4$ MW/m ($p = 5000$ Pa, $f = 0.5$ MHz; unbroken line T, line with symbols T_{ve}).

D. Comparison between the StS and the MT predictions

This section compares the predictions obtained by the StS and MT NLTE models. Figure 9 shows the comparison in terms of temperatures and N mole fraction. For both the StS and MT solutions, decreasing the pressure has the effect of enhancing thermal non-equilibrium. In the case of the MT model, the translational-rotational temperature is maximum on the axis and decreases monotonically when approaching the wall.

On the other hand the free-electron temperature increases, reaches a maximum and then decreases until it reaches the value determined from the adiabatic bound-

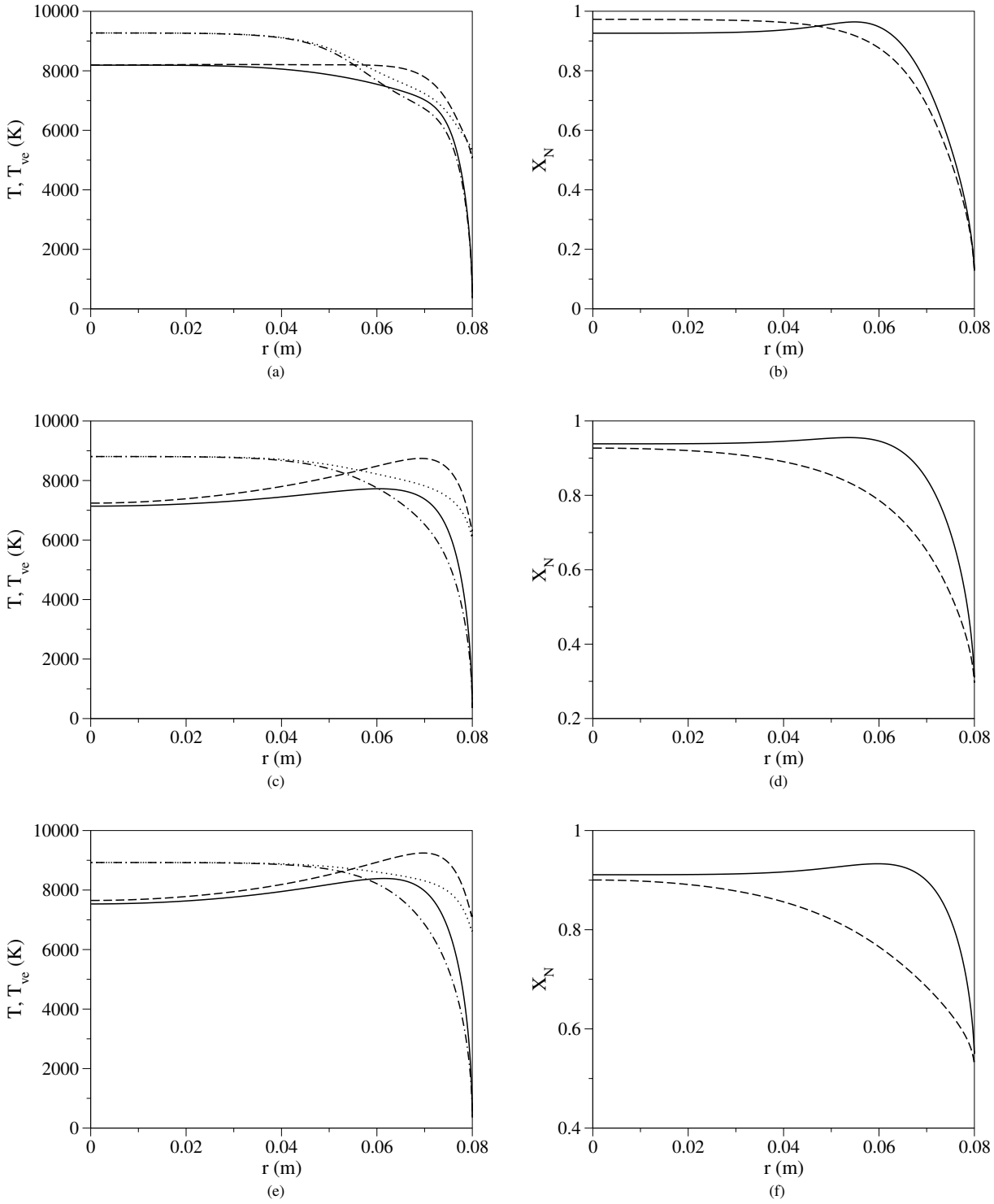

FIG. 9. Comparison between the translational-rotational temperature (left) and the N mole fraction (right) distributions predicted by the StS and the MT NLTE models at different pressures: (a)-(b) $p = 10\,000\,\mathrm{Pa}$, (c)-(d) $p = 5000\,\mathrm{Pa}$, (e)-(f) $p = 3000\,\mathrm{Pa}$ ($f = 0.5\,\mathrm{MHz}$, $P_0 = 0.35\,\mathrm{MW/m}$; in (a), (c) and (e) unbroken line T StS, dashed line T_{ve} StS, dotted-dashed line T MT, dotted line T_{ve} MT; in (b), (d) and (f) unbroken line StS, dashed line MT).

ary condition. This behavior is due to the balance between the Joule heating (which heats up the electron gas) and the energy loss in elastic and inelastic collisions, and chemical reactions. The peak location of the free-electron temperature moves towards the wall when decreasing the pressure. This is a consequence of the Joule heating dis-

tribution (not shown in Fig. 9) which becomes sharper and clustered to the wall at lower pressures. It is worth noticing that, in the StS simulation, (i) the translational-rotational temperature no longer exhibits a monotone behavior and (ii) the axis values of both temperatures are systematically lower than those predicted by the MT model. The differences observed between the StS and MT temperature distribution have an effect, as it should be expected, on the chemical composition (see Figs. 9(b), 9(d) and 9(f)).

Figure 10 shows the normalized population of the electronic levels of N on the torch axis (circles), in the midpoint of the torch (squares) and at the wall (triangles) at different pressures. The population exhibit significant distortions from a Boltzmann shape only close to the wall (where recombination occurs). Deviations from a Boltzmann distributions are more significant when increasing the pressure due to higher recombination.

V. CONCLUSIONS

A tightly coupled magneto-hydrodynamic solver for the study of the weakly ionized plasmas found in RF discharges has been developed. A hierarchy of thermophysical models have been added to the solver to model the non-equilibrium effects in atomic and molecular plasmas. These include LTE, multi-temperature and the more sophisticated State-to-State models. The governing equations for the flow and electromagnetic fields have been written as a system of coupled time-dependent conservation-laws. Steady-state solutions have been obtained by means of an implicit Finite Volume Method.

Results obtained by using a multi-temperature and State-to-State models have shown that the LTE assumption does not hold and that its use can lead to a wrong prediction of the thermo-chemical state of the gas. The analysis of the temperature distribution in the torch indicated that non-equilibrium plays an important role close to the walls, due to the combined effects of Ohmic heating, and chemical composition and temperature gradients. The accurate study of the population of excited electronic states has shown that, in view of the absence of a macroscopic gas flow, non-Boltzmann distributions are limited to a narrow region close to the torch wall.

ACKNOWLEDGMENTS

Research of A. Munafò was supported by the University of Illinois at Urbana-Champaign Starting Grant. Research of M. Panesi and S. A. Alfuhaid was supported by the AFOSR Summer Faculty Fellowship Program. Research of J.-L. Cambier was sponsored by AFOSR grant 14RQ13COR (PM: M. Birkan).

[1] M. I. Boulos, Pure & Appl. Chem. **9**, 1321 (1985).
[2] J. Mostaghimi and M. I. Boulos, in *Inductively Coupled Plasma in Analytical Spectrometry* (1992) pp. 949–984.

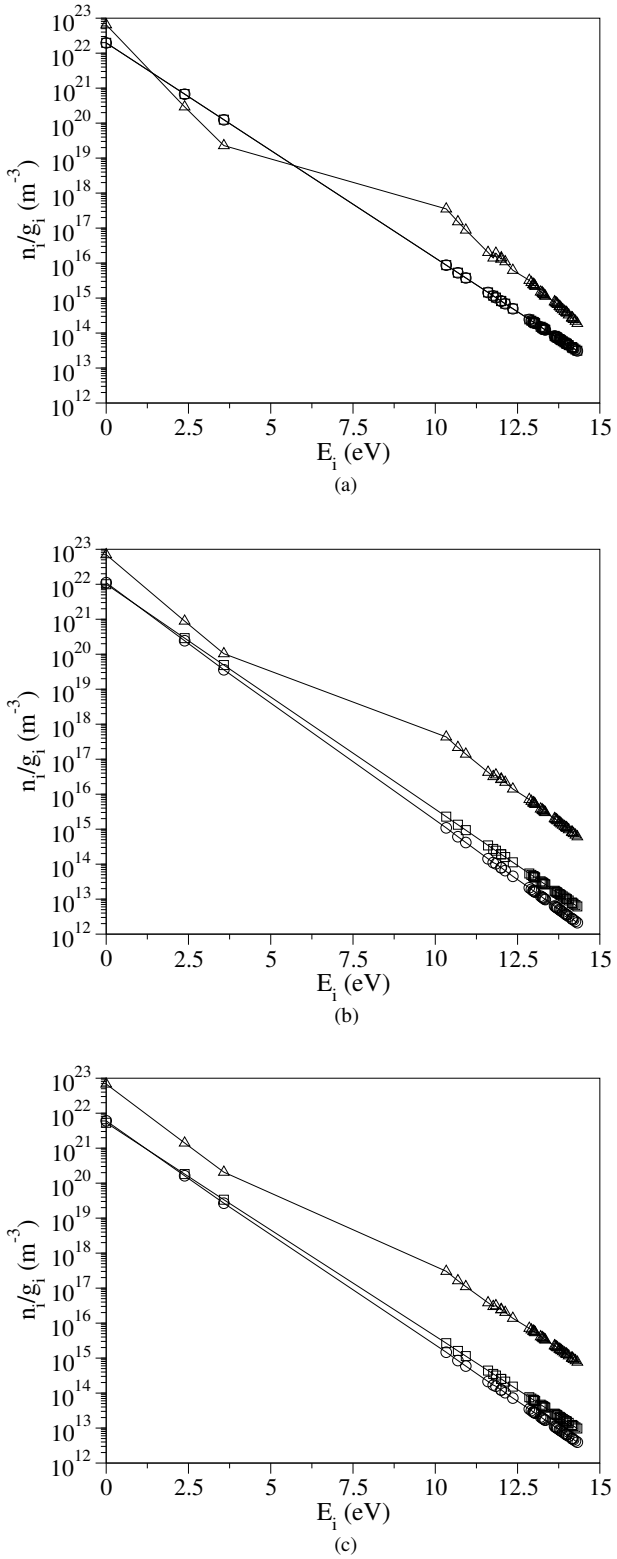

FIG. 10. Normalized population of the electronic levels of N at different pressures: (a) $p = 10\,000\,\mathrm{Pa}$, (b) $p = 5000\,\mathrm{Pa}$, (c) $p = 3000\,\mathrm{Pa}$ ($f = 0.5\,\mathrm{MHz}$, $P_0 = 0.35\,\mathrm{MW/m}$; line with circles $r = 0\,\mathrm{m}$ [axis], line with squares $r = 0.04\,\mathrm{m}$, line with triangles $r = 0.08\,\mathrm{m}$ [wall]).

[3]T. B. Reed, J. Appl. Phys. **32**, 821 (1961).

[4]D. Giordano, "Hypersonic-flow governing equations with electromagnetic fields," AIAA Paper 2002–2165 (2002) 33rd Plasmadynamics and Lasers Conference, Maui, HW.

[5]T. G. Cowling, *Magnetohydrodynamics*, Monographs on Astronomical Subjects (Hilger, London, 1976).

[6]D. V. Abeele, *An Efficient Computational Model for Inductively Coupled Air Plasma Flows Under Thermal and Chemical Non-Equilibrium*, Ph.D. thesis, Univesité Libre de Bruxelles, Bruxelles, Belgium (2000).

[7]M. P. Freeman and J. C. Chase, J. Appl. Phys. **39**, 180 (1968).

[8]D. R. Keefer, J. A. Sprouse, and F. C. Loper, IEEE Trans. Plasma Sci. **1**, 71 (1973).

[9]H. U. Eckert, J. Appl. Phys. **41**, 1520 (1970).

[10]H. U. Eckert, J. Appl. Phys. **41**, 1529 (1970).

[11]H. U. Eckert, J. Appl. Phys. **43**, 46 (1972).

[12]H. U. Eckert, J. Appl. Phys. **48**, 1467 (1977).

[13]B. Shaw., J. Appl. Phys. **99**, 034906 (2006).

[14]J. J. Thompson, Phil. Mag. **4**, 1128 (1927).

[15]A. N. Tikhonov and A. A. Samarskii, *Equations of Mathematical Physics*, Dover Books on Physics (Dover Publications, Mineola, NY, 1990).

[16]D. C. Pridmore-Brown, J. Appl. Phys. **41**, 3621 (1970).

[17]M. I. Boulos, IEEE Trans. Plasma Sci. **1**, 28 (1976).

[18]J. Mostaghimi, P. Proulx, and M. I. Boulos, Plasma Chem. Plasma Process. **3**, 199 (1984).

[19]J. Mostaghimi and P. P. M. I. Boulos, Num. Heat Transfer **2**, 187 (1985).

[20]J. Mostaghimi, P. Proulx, and M. I. Boulos, J. Appl. Phys. **61**, 1753 (1987).

[21]P. Proulx, J. Mostaghimi, and M. I. Boulos, Plasma Chem. Plasma Process. **1**, 29 (1987).

[22]J. Mostaghimi and M. I. Boulos, J. Appl. Phys. **68**, 2643 (1990).

[23]R. Ye, P. Proulx, and M. I. Boulos, Int. J. Heat Mass Transfer **42**, 1585 (1999).

[24]A. F. Kolesnikov, in *Proc. of the 2nd ESA Symposium on Aerothermodynamics for Space Vehicles* (ESA Publication Div., The Netherlands, 1994) pp. 583–588.

[25]A. F. Kolensikov, in *Physico-Chemical Models for High Enthalpy and Plasma Flows*, Lecture Series (von Karman Institute for Fluid Dynamics, 1999).

[26]S. A. Vasil'evskii and A. F. Kolesnikov, Fluid Dyn. **35**, 769 (2000).

[27]N. G. Bykova, S. A. Vasilevskii, and A. F. Kolesnikov, High Temp. **42**, 12 (2004).

[28]A. N. Gordeev, A. F. Kolesnikov, and Y. K. Rulev, in *Proc. of the 5th ESA Symposium on Aerothermodynamics for Space Vehicles* (ESA Publication Div., The Netherlands, 2005) pp. 164–170.

[29]P. Rini, A. F. Kolesnikov, S. A. Vasil'evskii, O. Chazot, and G. Degrez, "CO_2 stagnation line flow simulation for mars entry applications," AIAA Paper 2005–5206 (2007) 38th AIAA Thermophysics Conference, Toronto, Canada.

[30]A. N. Gordeev and A. F. Kolesnikov, High Temp. **45**, 506 (2010).

[31]X. Chen and E. Pfender, Plasma Chem. Plasma Process. **1**, 103 (1991).

[32]D. V. Abeele and G. Degrez, AIAA Journal **38**, 234 (2000).

[33]M. Panesi, P. Rini, G. Degrez, and O. Chazot, J. Thermophys. Heat Transfer **21**, 57 (2007).

[34]M. E. Morsli and P. Proulx, J. Phys. D: Appl. Phys **40**, 4810 (2007).

[35]R. C. Miller and R. J. Ayen, J. Appl. Phys. **40**, 5260 (1969).

[36]For fixed values of the elemental fractions.

[37]W. Zhang, A. Lani, H. B. Chew, and M. Panesi, "Modeling of non-equilibrium plasmas in an inductively coupled plasma facility," AIAA Paper 2014–2235 (2014) 45th AIAA Plasmadynamics and Lasers Conference, Atlanta, GA.

[38]J.-L. Cambier and S. Moreau, "Simulation of a molecular plasma in collisional-radiative nonequilibrium," AIAA Paper 1993–3196 (1993) 24th Plasmadynamics and Laser Conference, Orlando, FL.

[39]M. Capitelli, I. Armenise, D. Bruno, M. Cacciatore, R. Celiberto, G. Colonna, O. D. Pascale, P. Diomede, F. Esposito, C. Gorse, K. Hassouni, A. Laricchiuta, S. Longo, D. Pagano, D. Pietanza, and M. Rutigliano., "Non-equilibrium plasma kinetics: a state-to-state approach," Plasma sources, science and technology (2006) 8th European Sectional Conference on Atomic and Molecular Physics of Ionized Gases.

[40]A. Bultel, B. van Ootegem, A. Bourdon, and P. Vervisch, Phys. Rev. E **65**, 046406 (2002).

[41]Y. Liu, M. Vinokur, M. Panesi, and T. E. Magin, "A multi-group maximum entropy model for thermo-chemical nonequilibrium," AIAA Paper 2010–4332 (2010) 10th AIAA/ASME Joint Thermophysics and Heat Transfer Conference, Chicago, IL.

[42]Y. Liu, M. Panesi, M. Vinokur, and P. Clarke, "Microscopic simulation and macroscopic modeling of thermal and chemical non-equilibrium gases," AIAA Paper 2013–3146 (2013) 44th AIAA Thermophysics Conference, San Diego, CA.

[43]A. Bultel, B. G. Chéron, A. Bourdon, O. Motapon, and I. F. Schneider, Phys. Plasmas **13**, 043502 (2006).

[44]M. Panesi, T. E. Magin, A. Bourdon, A. Bultel, and O. Chazot, J. Thermophys. Heat Transfer **23**, 236 (2009).

[45]M. Panesi, T. E. Magin, A. Bourdon, A. Bultel, and O. Chazot, J. Thermophys. Heat Transfer **25**, 361 (2011).

[46]A. Munafò, A. Lani, A. Bultel, and M. Panesi, Phys. Plasmas **20**, 073501 (2013).

[47]M. Panesi, R. L. Jaffe, D. W. Schwenke, and T. E. Magin, J. Chem. Phys **138**, 044312 (2013).

[48]A. Munafò, M. Panesi, and T. E. Magin, Phys. Rev. E **89**, 023001 (2014).

[49]M. Panesi, A. Munafò, T. E. Magin, and R. L. Jaffe, Phys. Rev. E **90**, 013009 (2014).

[50]H. P. Le, A. P. Karagozian, and J.-L. Cambier, Phys. Plasmas **20**, 123304 (2013).

[51]F. Esposito and M. Capitelli, Chem. Phys. Lett. **302**, 49 (1999).

[52]F. Esposito, I. Armenise, and M. Capitelli, Chem. Phys. **331**, 1 (2006).

[53]D. W. Schwenke, in *Non-Equilibrium Gas Dynamics - From Physical Models to Hypersonic Flights*, Lecture Series (von Karman Institute for Fluid Dynamics, 2008).

[54]R. L. Jaffe, D. W. Schwenke, G. Chaban, and W. Huo, "Vibrational and rotational excitation and relaxation of nitrogen from accurate theoretical calculations," AIAA Paper 2008–1208 (2008) 46th AIAA Aerospace Sciences Meeting and Exhibit, Reno, NV.

[55]G. Chaban, R. L. Jaffe, D. W. Schwenke, and W. Huo, "Dissociation cross-sections and rate coefficients for nitrogen from accurate theoretical calculations," AIAA Paper 2008–1209 (2008) 46th AIAA Aerospace Sciences Meeting and Exhibit, Reno, NV.

[56]R. L. Jaffe, D. W. Schwenke, and G. Chaban, "Theoretical analysis of N_2 collisional dissociation and rotation-vibration energy transfer," AIAA Paper 2009–1569 (2009) 47th AIAA Aerospace Sciences Meeting and Exhibit, Orlando, FL.

[57]I. V. Adamovich, S. O. Macheret, J. W. Rich, and C. E. Treanor, AIAA J. **33**, 1064 (1995).

[58]I. V. Adamovich, S. O. Macheret, J. W. Rich, and C. E. Treanor, AIAA J. **33**, 1070 (1995).

[59]C. Park, J. Thermophys. Heat Transfer **3**, 233 (1989).

[60]C. Park, J. Thermophys. Heat Transfer **7**, 385 (1993).

[61]C. Park, J. T. Howe, R. L. Jaffe, and G. V. Candler, J. Thermophys. Heat Transfer **8**, 9 (1994).

[62]C. Park, R. L. Jaffe, and H. Partridge, J. Thermophys. Heat Transfer **15**, 76 (2001).

[63]E. Josyula, W. F. Bailey, and S. M. Ruffin, Phys. Fluids **15**, 3223 (2003).

[64]M. Panesi and A. Lani, Phys. Fluids **25**, 057101 (2013).

[65]M. G. Kapper and J.-L. Cambier, J. Appl. Phys. **109**, 113308 (2011).

[66]M. G. Kapper and J.-L. Cambier, J. Appl. Phys. **109**, 113309 (2011).

[67]A. Munafò, M. G. Kapper, J.-L. Cambier, and T. E. Magin, "Investigation of nonequilibrium effects in axisymmetric nozzle and

blunt body nitrogen flows by means of a reduced rovibrational collisional model," AIAA Paper 2012–0647 (2012) 50h AIAA Aerospace Sciences Meeting including the New Horizons Forum and Aerospace Exposition, Nashville, TN.
[68]C. Hirsch, *Numerical Computation of Internal and External Flows* (John Wiley & Sons, New York, NY, 1990).
[69]M. Capitelli, C. M. Ferreira, B. F. Gordiets, and A. I. Osipov, *Plasma Kinetics in Atmospheric Gases* (Springer, 2000).
[70]L. Pauling and E. B. Wilson Jr., *Introduction to Quantum Mechanics with Applications to Chemistry*, Dover Books on Physics (Dover Publications, Mineola, NY, 1985).
[71]L. V. Gurvich, *Thermodynamic Properties of Individual Substances* (CRC press, 1994).
[72]V. Giovangigli, *Multicomponent Flow Modeling* (Birkhäuser, Berlin, 1999).
[73]E. Nagnibeda and E. Kustova, *Non-Equilibrium Reacting Gas Flows* (Springer, Berlin, 2009).
[74]L. Landau and E. Teller, Phys. Z Sowjetunion **10**, 34 (1936), in German.
[75]G. V. Candler and R. W. MacCormack, J. Thermophys. Heat Transfer **5**, 266 (1991).
[76]A. Bourdon and P. Vervisch, Phys. Rev. E **52**, 1888 (1996).
[77]J. H. Ferziger and H. G. Kaper, *Mathematical Theory of Transport Processes in Gases* (North-Holland Pub. Co., 1972).
[78]R. S. Devoto, Phys. Fluids **9**, 1230 (1966).
[79]T. E. Magin and G. Degrez, Phys. Rev. E **70**, 046412 (2004).
[80]V. Giovangigli, IMPACT Comput. Sci. Eng. **2**, 73 (1990).
[81]T. E. Magin and G. Degrez, J. Comput. Phys. **198**, 424 (2004).
[82]A. Munafò and T. E. Magin, Phys. Fluids **26**, 097102 (2014).
[83]K. L. Heritier, R. L. Jaffe, V. Laporta, and M. Panesi, J. Chem. Phys. **141**, 184302 (2014).